Atmos. Chem. Phys. Discuss., 13, 18749–18770, 2013
www.atmos-chem-phys-discuss.net/13/18749/2013/
doi:10.5194/acpd-13-18749-2013

Atmospheric Chemistry and Physics Discussions

Radiative consequences of low-temperature infrared refractive indices for supercooled water clouds

P. M. Rowe[1], **S. Neshyba**[2], **and V. P. Walden**[1]

[1]Department of Geography, University of Idaho, 875 Perimeter Drive, Moscow, ID, 83844, USA
[2]Department of Chemistry, University of Puget Sound, 1500 N. Warner, Tacoma, WA, 98416, USA

Received: 26 April 2013 – Accepted: 21 June 2013 – Published: 12 July 2013

Correspondence to: P. M. Rowe (prowe@harbornet.com)

Published by Copernicus Publications on behalf of the European Geosciences Union.

Abstract

Simulations of cloud radiative properties for climate modeling and remote sensing rely on accurate knowledge of the complex refractive index (CRI) of water. Although conventional algorithms employ a temperature independent assumption (TIA), recent infrared measurements of supercooled water have demonstrated that the CRI becomes increasingly ice-like at lower temperatures. Here, we assess biases that result from ignoring this temperature dependence. We show that TIA-based cloud retrievals introduce spurious ice into pure, supercooled clouds, or underestimate cloud thickness and droplet size. TIA-based downwelling radiative fluxes are lower than those for the temperature-dependent CRI by as much as $1.7\,\mathrm{W\,m^{-2}}$ (in cold regions), while top-of-atmosphere fluxes are higher by as much as $3.4\,\mathrm{W\,m^{-2}}$ (in warm regions). Proper accounting of the temperature dependence of the CRI, therefore, leads to significantly greater local greenhouse warming due to supercooled clouds than previously predicted. The current experimental uncertainty in the CRI at low temperatures must be reduced to properly account for supercooled clouds in both climate models and cloud property retrievals.

1 Introduction

Clouds represent an important source of uncertainty in radiative flux, and therefore climate (IPCC, 2007). Supercooled water clouds occur globally, e.g. (Intrieri, 2006; Verlinde et al., 2007; Hogan et al., 2003; Hu et al., 2010; Zhang et al., 2010; Rosenfeld and Woodsley, 2000). Recent work finds that midlevel supercooled-liquid topped stratiform clouds make up 33.6 % of midlevel clouds (Zhang et al., 2010). In the Arctic, ubiquitous supercooled liquid cloud is a significant driver of radiative flux (Cesana et al., 2012).

Radiative properties of supercooled clouds depend on microphysical properties (particle size and shape), as well as complex refractive index (CRI) spectra, over the full

ACPD
13, 18749–18770, 2013

range of supercooled temperatures from freezing to the homogeneous freezing point of 235 K (Koop et al., 2000).

Figure 1a and b shows that the infrared CRI of thermodynamically stable water (henceforth "water") is different from that of ice in key regions (Hale and Querry, 1973; Downing and Williams, 1975; Bertie and Lan, 1996; Warren and Brandt, 1994; Toon et al., 1994). For water, a prominent absorption peak appears at 600 cm^{-1} in the imaginary part of the CRI; in ice, a similar peak appears at $\sim$ 800 cm^{-1}. This shift plays a key role in phase discrimination using infrared remote sensing. While the CRI of ice varies significantly with temperature, that of water (for temperatures > 273 K) does not. This provides a measure of justification for the temperature-independent assumption (TIA) for water above 273 K. However, the TIA is also widely used at temperatures below 273 K.

Recent CRI of supercooled water (Zasetsky et al., 2005; Wagner et al., 2005) are shown in Fig. 1c and d. The CRI of supercooled water is distinctly temperature dependent and is intermediate between liquid and ice. (This behavior is attributed to low density, ice-like domains in supercooled water (Zasetsky et al., 2004).) In light of this temperature dependence, it is important to assess the effect of the TIA on remote sensing retrievals and climate modeling.

In this paper, we compare simulated fluxes from supercooled liquid water clouds using the CRI of Downing and Williams (1975), based on measurements made at 300 K, to simulated fluxes using temperature-dependent CRI based on relatively recent measurements of Zasetsky et al. (2005) and Wagner et al. (2005) at temperatures of 273 K to 240 K. In addition, we estimate errors in cloud property retrievals from downwelling infrared radiance spectra for the TIA. Simulations are performed for single-layer liquid only clouds, for a variety of atmospheric and cloud conditions and for both downwelling radiance/flux at the surface and upwelling radiance/flux at the top of atmosphere (TOA). In Sect. 2, we discuss the creation of a temperature-dependent complex CRI for supercooled liquid water, which is a hybrid that uses the best measurements of both Zasetky et al. and Wagner et al. (2005). Section 3 gives the methods, including simulating radi-

ACPD
13, 18749–18770, 2013

ances and fluxes and determining the spectral regions to use for the analysis. Section 4 discusses sources of error in the flux calculations. In Sect. 5, we present and discuss flux differences between simulations using the CRI of Downing and Williams (1975) and using the temperature-dependent CRI in two infrared spectral regions where clouds have a large signal and where the temperature-dependence of the CRI appear to be well known: 460 to 640 cm^{-1} and 740 to 990 cm^{-1}. Section 6 presents conclusions.

2 A new CRI for supercooled water

The measurements of Zasetsky et al. (2005) extend from 460 to 6000 cm^{-1} while those of Wagner et al. (2005) extend from 800 to 6000 cm^{-1}. From 800 to 1000 cm^{-1} the imaginary parts of the CRI (k-spectra) are typically within about 7 % of each other. At wavenumbers below 800 cm^{-1}, near the peak in k, errors in Zasetsky et al. (2005) are expected to be $\sim$ 1.5 %, while from 1000 to 1300 cm^{-1}, where k is small, errors are large, rendering the refractive indices unusable. These large errors explain the poor agreement from 1000 to 1300 cm^{-1} between the 273 K indices of Zasetsky et al. (2005) and other indices (Fig. 1d; note that the solid magenta line is well below the other curves). By contrast, the method of Wagner et al. (2005) resulted in smaller errors in regions where k is small. However, from 1000 to 1300 cm^{-1}, even the uncertainties in the k-spectra of Wagner et al. (2005) are likely to be larger than the temperature dependence.

Based on these considerations, a new temperature-dependent set of refractive indices at temperatures of 240, 253, 263 and 273 K was created. From 460 to 800 cm^{-1}, the new refractive indices are identical to the measurements of Zasetsky et al. (2005). From 800 to 1000 cm^{-1} they are intermediate between those of Zasetsky et al. (2005) and Wagner et al. (2005), changing linearly from the value measured by Zasetsky et al. (2005) at 800 cm^{-1} to the value measured by Wagner et al. (2005) at 1000 cm^{-1}. From 1000 to 1400 cm^{-1}, the measurements of Wagner et al. (2005) are used. Because the measurements of Wagner et al. (2005) were made at different tem-

ACPD
13, 18749–18770, 2013

peratures (238, 252, 258, and 269 K), they were first interpolated to the temperatures of Zasetsky et al. (2004).

3 Methods

3.1 Simulations of radiance and spectral flux

Radiances and spectral fluxes for supercooled liquid clouds were simulated as follows (more detail is given in the Supplement). Single-scattering parameters were created from the CRI using Mie theory. Atmospheric profiles were created for tropical, mid-latitude summer, Arctic summer, mid-latitude winter, and Arctic winter and inputted to the Line-By-Line Radiative Transfer Model (LBLRTM; Clough et al., 2005) to get gaseous optical depths. Finally, downwelling and upwelling radiances and spectral fluxes were calculated using a program for DIScrete-Ordinate-method Radiative Transfer in scattering and emitting layered media (DISORT; Stamnes et al., 1988), for each atmospheric profile (e.g. set of gaseous optical depths and temperature profile) and for a variety of liquid cloud effective radii and liquid water paths (LWPs).

Simulations were performed both for the TIA and for temperature-dependent CRI. For the TIA, the single-scattering parameters for the CRI measurements of Downing and Williams for 300 K were used regardless of cloud temperature. For simulations using the temperature-dependent CRI, the single-scattering parameters used depended on cloud temperature; single-scattering parameters for CRI at temperatures above and below cloud temperature were linearly interpolated to the cloud temperature.

3.2 Choice of wavenumbers

The infrared spectral regions at which supercooled clouds have the greatest radiative effect depend on geographic location as well as the direction of flux (upward or downward). In order to select spectral regions that are sensitive to clouds and where

ACPD
13, 18749–18770, 2013

the temperature dependence of the CRI is known, we focus on two extreme atmospheres: cold/dry and warm/wet (Arctic winter and tropical atmospheres; see Supplement) and examine downwelling infrared spectral fluxes as they would be measured by an upward-looking instrument at the surface, and upwelling infrared spectral fluxes as they would be measured by a downward-looking instrument at the top of the atmosphere.

Simulated clear-sky upwelling and downwelling flux spectra for the extreme atmospheres are compared to simulated cloudy-sky spectra, for single-layer liquid clouds with LWPs of 8 g m^{-2} and an effective radius (r_e) of 10 µm, placed at heights such that the cloud temperature is 240 K; 240 K was chosen to explore the extreme low of CRI measurements. These comparisons are used to determine the spectral regions where the effect of supercooled water clouds dominates.

Figure 2a shows simulated upwelling spectral fluxes. From about 460 to 600 cm^{-1} (the "dirty window") and 800 to 1250 cm^{-1} (the "atmospheric window") absorption from trace gases is weak, so most of the surface flux is transmitted to the TOA. The effect of a tropical cloud (compare red solid curve to pink dashed curve) is considerable because the cloud (240 K) is much colder than the surface (300 K). By contrast, for Arctic winter clouds, there is little difference in temperature between cloud (240 K) and surface (238 K; a temperature inversion is present), so the cloud has little effect (compare solid blue curve to dashed light blue curve). Thus, for upwelling flux, the greatest sensitivity to supercooled cloud content occurs in warm, wet atmospheres, in the window regions.

Figure 2b shows simulated downwelling spectral fluxes. The clear-sky Arctic winter spectral flux is low in the window regions due to weak trace gas emission. The tropical clear-sky spectrum is more "filled in" than that of the Arctic winter, due to emission from water vapor in the warm, humid atmosphere. The dirty window is completely filled in, and thus there is no increase in downwelling radiances for the cloudy tropical case. For both atmospheres, clouds cause an increase in downwelling radiance in the atmospheric window, but the increase is considerably greater in the Arctic winter. Thus for

ACPD
13, 18749–18770, 2013

downwelling flux, the greatest sensitivity to supercooled cloud content occurs in cold, dry atmospheres, in the window regions.

Because clouds have little effect between 640 and 760 cm^{-1} and 1250 to 2000 cm^{-1} (due to strong absorption and emission by water vapor and CO_2), and from 990 to 1050 cm^{-1} (due to O_3), we exclude these regions from the spectral flux calculations used to determine flux differences for the TIA. From 1050 to 1250 cm^{-1} relative uncertainties in the CRI are large and the temperature dependence of the CRI is not well characterized (see Supplement) so we exclude this spectral region from the flux calculations. However, this region is important for clouds, and higher accuracy CRI measurements from 235 to 273 K are thus crucial for a complete understanding of the infrared radiative transfer of supercooled liquid clouds. The wavenumber regions used in this study are, therefore, from 460 to 640 cm^{-1} and 760 to 990 cm^{-1}.

3.3 Flux differences

To determine biases in fluxes due to the TIA, spectral fluxes (in $W(m^2\,cm^{-1})^{-1}$) were integrated over 460 to 640 cm^{-1} and 760 to 990 cm^{-1} and summed to get a flux (in $W\,m^{-2}$). The flux for the TIA was then subtracted from the flux determined using the temperature-dependent CRI to give the flux difference.

3.4 Cloud-property retrievals

To determine errors in retrieved cloud properties due to the TIA, we perform cloud-property retrievals from model downwelling infrared radiances as follows. A set of model clouds are specified according to desired a priori cloud properties. For each such cloud, we create a zenith-view downwelling radiance spectrum, R_T, using CRI that depend on the cloud temperature. The wavenumbers at which these radiances are calculated lie between strong lines of gaseous emission, as described previously. We then create a set of simulated radiance spectra, R_{TIA}, for a variety of cloud properties. The difference between R_T and the R_{TIA} at the selected wavenumbers is then

ACPD
13, 18749–18770, 2013

calculated. The retrieved cloud properties are defined to be those that give rise to the minimum root mean square of this difference. These retrieved cloud properties can then be compared to the a priori cloud properties to get biases due to the TIA.

4 Sources of error

Sources of error in the radiances and fluxes calculated by DISORT include uncertainties in the liquid-water CRIs and in the single-scattering parameters created from them, error in the DISORT calculations, error due to omitting the atmosphere above a certain altitude, and error due to sampling the optical depths on a finite wavenumber grid. Errors in clear-sky optical depths are omitted from the analysis because the atmospheric profiles are meant to be typical examples only, rather than exact, and thus uncertainties in them and errors due to the atmospheric modeling of LBLRTM need not be considered; furthermore, such uncertainties do not depend on refractive indices and thus have only a small effect on radiances and flux differences. Uncertainties in the CRIs are probably the most important sources of error and the most difficult to quantify. To minimize other errors, we choose the output wavenumbers and atmospheric layers carefully, as described below. These errors can be roughly estimated by assuming clear-sky LBLRTM calculations, which are calculated line-by-line and are finely sampled in wavenumber, for an atmospheric model extending from 0 to 60 km, represent "truth," and comparing them to DISORT simulations with negligible cloud amount.

4.1 Uncertainties in CRI

Uncertainties in CRI are not well known. We assume an uncertainty of 4 % in the CRI of Downing and Williams (1975), based on the difference between these CRIs and those of Bertie and Lan (1996) and Hale and Querry (1973) within 460 to 640 and 740 to 990 cm^{-1}: 1 % for the real part and 4 % for the imaginary part, on average. The uncertainties in the measurements by Zasetsky et al. (2005) and Wagner et al.

ACPD
13, 18749–18770, 2013

(2005) are not well known. We use the comparison between the two sets between 800 and 930 cm^{-1} to get estimates of the error: differences are 5, 3, 6, and 8 % for the 273 K, 263 K, 253 K, and 240 K measurements, respectively. Combined uncertainties for Downing and Williams (1975) vs. the new temperature-dependent CRIs are then 6, 5, 7, and 9 % for 273 K, 263 K, 253 K, and 240 K.

Note that the new temperature-dependent CRI are created from interpolating the real and imaginary parts separately. A rigorous treatment would be to recalculate the real part of the CRI from the imaginary part using the Kramers–Kronig transform. However, any errors in the real part of the CRI due to this method should be smaller than errors in the measurements of Zasetsky et al. (2005) and Wagner et al. (2005), from which they are derived.

Since the 273 K CRI is, on average, 18 % different than the 300 K CRI, up to 30 % (6 % out of 18 %) of the flux difference observed for 273 K clouds could be accounted for by errors in measured indices. Similarly, since indices measured at 263 K, 253 K, and 240 K differ from the 300 K indices by 21, 32, and 47 %, uncertainty estimates made in this manner are 20 %. Similarly, uncertainties in cloud property retrievals are estimated to be about 20 %.

4.2 Error in DISORT calculations

Error in DISORT calculations is due, in part, to the assumption that the Planck function is linear in optical depth across a layer. Errors due to this approximation can be minimized by making layers thin, so that the temperature difference across a layer is small. However, a sensitivity study showed that the accuracy of DISORT calculations is poor for layer optical depths less than 10^{-5}. Thus layers need to be thick enough to have an adequately thick optical depth, but thin enough to have a small temperature gradient. We carefully choose atmospheric layers such that the temperature differential across layers is < 5 K up to 10 km and < 10 K up to 60 km.

Errors in the DISORT flux calculations are estimated to range, for Arctic winter (AW) to tropical (TRP) model atmospheres, from 0.005 to 0.02 $W\,m^{-2}$ for downwelling and

ACPD
13, 18749–18770, 2013

0.007 to 0.2 $W m^{-2}$ for upwelling. These represent the dominant sources of uncertainty in DISORT simulations of flux. Errors in DISORT calculations of radiances, used for cloud property retrievals, are expected to be negligible compared to error due to uncertainties in CRI.

Since these errors do not depend on CRI, they should cancel out to a large degree when flux and radiance differences are calculated.

4.3 Error due to choice of TOA

Even with careful choice of layering, at some wavenumbers optical depths below 10^{-5} occur at altitudes as low as 10 km, while at other wavenumbers (near strong line-centers), optical depths can still be large enough that the atmosphere above 30 km needs to be included for good accuracy. Thus, for each DISORT run (each wavenumber), the atmospheric profile was topped at the highest layer with an optical depth greater than 10^{-5}. This resulted in a wavenumber-dependent model TOA ranging from 8.5 to 60 km. Errors in fluxes due to excluding such small optical depths through truncating the atmosphere below 60 km are small; the range of resulting errors, for AW to TRP, is estimated to be 0.002 to 0.0007 $W m^{-2}$ for downwelling fluxes and 0.0002 to 0.001 $W m^{-2}$ for upwelling fluxes. Errors in radiances used for cloud-property retrievals are similarly small.

4.4 Error due to wavenumber sampling

Error due to sampling the optical depths on a finite wavenumber grid is minimized by selecting a fine wavenumber spacing (0.01 cm^{-1}) so that most strong gaseous lines are well-sampled for integrating over wavenumber. The LBLRTM calculates optical depths at perfect (monochromatic) resolution and outputs them on a spacing that becomes finer going up in the atmosphere (e.g. down to 2×10^{-4} cm^{-1} at 60 km). Because DISORT is run for each spectral point, running DISORT at the finest wavenumber sampling would take prohibitively long. The wavenumber spacing chosen represents that

ACPD
13, 18749–18770, 2013

of the lowest layer. The range of resulting errors, for AW to TRP, is estimated to be 0.0002 to 0.0003 W m^{-2} for downwelling and 0.003 to 0.006 W m^{-2} for upwelling fluxes. For cloud-property retrievals, error due to wavenumber sampling is negligible because strong gaseous emission lines are avoided.

4.5 Combined uncertainties

The combined uncertainties in the flux differences due to the choice of TOA and wavenumber sampling of the simulated fluxes are estimated to range, for AW to TRP, from 0.002 to 0.0007 W m^{-2} for downwelling and from 0.003 to 0.006 W m^{-2} for upwelling. Typically, the uncertainty in flux difference due to uncertainties in the measured CRIs (20 %) dominates over the other sources. For example, for a flux difference of 0.2 W m^{-2}, this would be ±0.04 W m^{-2}. For cloud-property retrievals, uncertainties in the measured CRIs dominate and the combined uncertainties are 20 % for cloud effective radius and LWP.

5 Results and discussion

5.1 Spectral fluxes

For a cloud at 240 K, simulated upwelling spectral fluxes are found to be biased high for the TIA (300 K CRI), compared to fluxes for the 240 K CRI, as shown in Fig. 3a for a tropical atmosphere. Simulated downwelling fluxes are biased low for the TIA (Fig. 3b; Arctic winter). Similar but smaller effects occur in the dirty window for both upwelling and downwelling. Figure 2 (introduced in the methods section), suggests that such biases are equivalent to underestimating cloudiness. Use of the TIA underestimates the local greenhouse effect of supercooled clouds.

ACPD
13, 18749–18770, 2013

5.2 Upwelling flux differences

Figure 4a and b shows the upwelling flux differences (flux (300 K CRI) – flux (240 K CRI)) as a function of LWP. The upwelling flux differences are positive and increase from the Arctic winter to the Tropics, in tandem with the cloud radiative effect (as was shown in Fig. 2). In addition, the flux differences decrease as r_e increases.

To understand the change in upwelling flux differences with LWP, it is helpful to think of the cloud radiative effect as being due to two processes, both of which reduce the upwelling flux and both of which depend on the LWP and CRI. The first is absorption of warm surface emission by the cloud and re-emission at the cloud temperature, which depends on the imaginary part of the CRI. For the tropical atmosphere, for small LWP, cloud absorption and emission increase with cloud thickness as LWP increases, and there is a corresponding increase in flux differences up to LWP = 8 g m^{-2}. For LWP > 8 g m^{-2}, the cloud becomes so optically thick that emission approaches a temperature-dependent maximum, depending less on the CRI, so that flux differences decrease with LWP.

The second process reducing the upwelling flux is multiple scattering by the cloud. It is best seen in the Arctic winter case (lowest curves of Fig. 4a and b), where the first process, absorption and emission by the cloud, plays a small role, since the surface and cloud temperatures are quite similar. Multiple scattering, which depends on both the real and imaginary parts of the CRI, increases with LWP until reaching a maximum for optically thick clouds. This has important consequences for cloud modeling, since it implies that use of the TIA will cause biases in cloudy-sky flux for supercooled liquid clouds of any optical thickness.

The largest upwelling flux differences are for a 240 K tropical liquid cloud: 3.4 ± 0.7 W m^{-2} (r_e = 5 µm) and 1.8 ± 0.4 W m^{-2} (r_e = 10 µm).

ACPD
13, 18749–18770, 2013

5.3 Downwelling flux differences

Figure 4c and d shows downwelling flux differences. Trends are similar to those for upwelling, but the flux differences are negative, also consistent with underestimating the local greenhouse warming due to the cloud. The main qualitative difference is for optically thick clouds. For the Arctic winter downwelling flux, the flux differences drop to zero for large LWP because the reduction in downwelling flux due to scattering is almost exactly accounted for by scattering of surface radiation off the bottom of the cloud back to the surface, since surface and cloud are at similar temperatures. Furthermore, trace gases below the cloud mitigate the effect. For other atmospheres, the surface is warmer than the 240 K cloud, and the scattering causes a small dependence on the CRI for optically thick clouds.

The largest-magnitude downwelling flux differences are for the Arctic winter 240 K liquid cloud: $-1.6 \pm 0.3\,\mathrm{W\,m^{-2}}$ ($r_e = 5\,\mu\mathrm{m}$) and $-0.95 \pm 0.2\,\mathrm{W\,m^{-2}}$ ($r_e = 10\,\mu\mathrm{m}$). These flux differences, and the flux differences of 3.4 and $1.8\,\mathrm{W\,m^{-2}}$ for tropical upwelling flux, are significant when compared to the total net anthropogenic global radiative forcing at the tropopause of 1.6 (−0.6; +0.24) $\mathrm{W\,m^{-2}}$ (Ramaswamy et al., 2001).

5.4 Cloud property retrievals

The use of the TIA also induces errors into retrievals of cloud properties that rely on infrared radiative transfer. Because the CRI of supercooled liquid water is more similar to ice than that for the TIA, cloud phase retrievals using the TIA retrieve an ice fraction that is biased high. For the downwelling radiance simulation for the Arctic winter (240 K liquid-only cloud), if the simulation is created using the temperature-dependent CRI, but the TIA is used for the retrieval, an ice fraction of ∼ 5 % is retrieved (see Fig. 5; the water path, $8\,\mathrm{g\,m^{-2}}$, and liquid r_e, 10 µm, are assumed to be known; the retrieved ice $r_e = 4\,\mu\mathrm{m}$). Thus, retrievals using the TIA may detect ice even if none is present. For a wider range of simulations (liquid r_e of 5 to 15 µm and LWP of 4 to $11\,\mathrm{g\,m^{-2}}$), use of the TIA leads to retrievals of ice fractions of 0 % to 12 %, with ice r_e of 1 to 10 µm.

ACPD
13, 18749–18770, 2013

(These ice r_e are small compared to estimates of ∼ 15 µm at 240 K for mid-latitude clouds, Garrett et al., 2003). If we assume that the cloud is known to be liquid-only, for the same cloud types, errors in retrieved r_e will be −3.2 to 0.5 µm and errors in LWP will be −2.3 to 0.6 g m^{-2}.

6 Conclusions

Supercooled clouds are important for the climate system globally. The infrared properties of such clouds depend on their complex refractive indices. Although recent measurements have been made of liquid cloud CRI down to temperatures as low as 240 K (Zasetsky et al., 2005; Wagner et al., 2005), calculations of flux from supercooled liquid clouds and retrievals of supercooled cloud properties that make use of infrared radiance measurements typically rely on CRI based on measurements at 273 K and above. We present biases in flux differences and cloud-property retrievals for supercooled liquid clouds when the CRI are assumed to be temperature independent. Flux differences were calculated for the spectral regions from 460 to 640 cm^{-1} and 760 to 990 cm^{-1}, where cloud signal is strong and where the temperature-dependence of the CRI is known. Cloud properties were retrieved in microwindows between strong gaseous emission lines in the same spectral region.

We find that flux simulations of 240 K supercooled single-layer liquid clouds (r_e of 5 to 10 µm) that use CRI for temperatures near 300 K lead to underestimation of the local cloud greenhouse effect. Compared to fluxes using new CRI for 240 K, downwelling infrared fluxes using the TIA are too low (0.2 to 1.7 W m^{-2}), with the largest effect in cold regions, and upwelling fluxes are too high (0.2 to 3.4 W m^{-2}), with the largest effect in warm regions. Furthermore, TIA-based retrievals of cloud properties introduce spurious ice, or underestimate cloud thickness and droplet size, depending on algorithm constraints.

Additional laboratory measurements are needed to confirm the recent measurements of CRI of supercooled water (Zasetsky et al., 2005; Wagner et al., 2005) and re-

ACPD
13, 18749–18770, 2013

duce uncertainties in measured CRI throughout the infrared. Meanwhile, climate models and cloud retrievals should use the new, temperature-dependent CRI for greatest accuracy.

Supplementary material related to this article is available online at: http://www.atmos-chem-phys-discuss.net/13/18749/2013/acpd-13-18749-2013-supplement.pdf.

Acknowledgements. We are grateful to A. F. Khalizov, R. Lynch, and T. C. Grenfell for helpful discussions. Support for this research came from the National Aeronautics and Space Administration (NASA) Research Opportunities in Space and Earth Science program (Contract NNX08AF79G) and from the National Science Foundation (NSF) Idaho Experimental Program to Stimulate Competitive Research (EPSCoR). SPN acknowledges support from the University of Puget Sound.

References

Bertie, J. E. and Lan, Z.: Infrared intensities of liquids XX: The intensity of the OH stretching band of liquid water revisited, and the best current values of the optical constants of H_2O(l) at 25 °C between 15,000 and 1 cm^{-1}, Appl. Spec., 50, 1047–1057, 1996. 18751, 18756

Cesana, G., Kay, J. E., Chepfer, H., English, J. M., and de Boer, G.: Ubiquitous low-level liquid-containing Arctic clouds: new observations and climate model constraints from CALIPSO-GOCCP, Geophys Res. Lett., 39, L20804, doi:10.1029/2012GL053385, 2012. 18750

Clough, S. A., Shephard, M. W., Mlawer, E. J., Delamere, J. S., Iacono, M. J., Cady-Pereira, K., Boukabara, S., and Brown, P. D.: Atmospheric radiative transfer modeling: a summary of the AER codes, J. Quant. Spectrosc. Radiat. Transf., 91, 233–244, 2005. 18753

Downing, H. D. and Williams, D.: Optical constants of water in the Infrared, J. Geophys. Res., 80, 1656–1661, 1975. 18751, 18753, 18756

ACPD
13, 18749–18770, 2013

Garrett, T. J., Gerber, H., Baumgardner, D. G., Twohy, C. H., and Weinstock, E. M.: Small, highly reflective ice crystals in low-latitude cirrus, Geophys. Res. Lett., 30, 2132, doi:10.1029/2003GL018153, 2003. 18762

Hale, G. M. and Querry, M. R.: Optical constants of water in the 200-nm to 200-mm region, Appl. Optics, 12, 1973. 18751, 18756

Hogan, R. J., Illingworth, A. J., O'Connor, E. J., and Baptista, J. P. V. P.: Characterisitics of mixed-phase clouds, II. A climatology from ground-based lidar, Q. J. Roy. Meteorol. Soc., 129, 2117–2134, 2003. 18750

Hu, Y., Rodier, S., Xu, K., Sun, W., Huang, J., Lin, B., Zhai, P., and Josset, D.: Occurrence, liquid water content, and fraction of supercooled water clouds from combined CALIOP/IIR/MODIS measurements, J. Geophys. Res., 115, D00H34, doi:10.1029/2009JD012384, 2010. 18750

Intrieri, J. M.: An annual cycle of Arctic surface cloud forcing at SHEBA, J. Geophys. Res., 107, 8030, doi:10.1029/2000JC000439, 2006. 18750

IPCC: Climate Change 2007: The Physical Science Basis, Contribution of Working Group I to the Fourth Assessment Report of the Intergovernmental Panel on Climate Change, edited by: Solomon, S., Qin, D., Manning, M., Chen, Z., Marquis, M., Averyt, K. B., Tignor, M., and Miller, H. L., Cambridge University Press, Cambridge, United Kingdom and New York, NY, USA, 2007. 18750

Koop, T., Luo, B., Tsias, A., and Peter, T.: Water activity as the determinant for homogenous ice nucleation in aqueous solutions, Nature, 406, 611–614, 2000. 18751

Ramaswamy, V., Boucher, O., Haigh, J., Hauglustaine, D., Haywood, J., Myhre, G., Nakajima, T., Shi, G. Y., Solomon, S., Bettsand, R., Charlson, R., Chuang, C., Daniel, J. S., Genio, A. D., van Dorland, R., Feichter, J., Fuglestvedt, J., de F. Forster, P. M., Ghan, S. J., Jones, A., Kiehl, J. T., Koch, D., Land, C., Lean, J., Lohmann, U., Minschwaner, K., Penner, J. E., Roberts, D. L., Rodhe, H., Roelofs, G. J., Rotstayn, L. D., Schneider, T. L., Schumann, U., Schwartz, S. E., Schwarzkopf, M. D., Shine, K. P., Smith, S., Stevenson, D. S., Stordal, F., Tegen, I., and Zhang, Y.: Radiative forcing of climate change. In: Climate Change 2001: The Scientific Basis, Contribution of Working Group I to the Third Assessment Report of the Intergovernmental Panel on Climate Change, edited by: Houghton, J. T., Ding, Y., Griggs, D. J., Noguer, M., van der Linden, P. J., Dai, X., Maskell, K., and Johnson, C. A., Cambridge University Press, Cambridge, UK and New York, NY, USA, 881 pp., 2001. 18761

Rosenfeld, D. and Woodsley, W. L.: Deep convective clouds with sustained supercooled liquid water down to −37.5 °C, Nature, 405, 440–442, 2000. 18750

ACPD
13, 18749–18770, 2013

Stamnes, K., Tsay, S.-C., Wiscomb, W., and Jayaweera, K.: Numerically stable algorithm for discrete-ordinate-method radiative transfer in multiple scattering and emitting layered media, Appl. Optics, 27, 2502–2509, 1988. 18753

Toon, O. B., Tolbert, M. A., Koehler, B. G., Middlebrook, A. M., and Jordan, J.: The infrared optical constants of H_2O-ice, amorphous acid solutions, and nitric acid hydrates, J. Geophys. Res., 99, 25631–25654, 1994. 18751

Verlinde, J., Harrington, J. Y., McFarqhar, G. M., Yannuzzi, V. T., Avramov, A., Greenberg, S., Johnson, N., Zhang, G., Poellot, M. R., Mather, J. H., Turner, D. D., Eloranta, E. W., Zak, B. D., Prenni, A. J., Daniel, J. S., Kok, G. L., Tobin, D. C., Holz, R., Sassen, K., Spangenberg, D., Minnis, P., Tooman, T. P., Ivey, M. D., Richardson, S. J., Bahrmann, C. P., Shupe, M., Demott, P. J., Heymsfield, A. J., and Schofield, R.: The mixed-phase Arctic cloud experiment, B. Am. Meteorol. Soc., 88, 205–221, doi:10.1175/BAMS-88-2-205, 2007. 18750

Wagner, R., Benz, S., Mhler, O., Saathoff, H., Schnaiter, M., and Schurath, U.: Mid-infrared extinction spectra and optical constants of supercooled water droplets, J. Phys. Chem. A, 109, 7099–7112, 2005. 18751, 18752, 18756, 18762

Warren, S. G. and Brandt, R. E.: Optical constants of ice from the ultraviolet to the microwave: a revised compilation, J. Geophys. Res., 113, D14220, doi:10.1029/2007JD009744, 1994. 18751

Zasetsky, A. Y., Khalizov, A. F., and Sloan, J. J.: Local order and dynamics in supercooled water: a study by IR spectroscopy and molecular dynamic simulations, J. Chem. Phys., 121, 6941–6947, 2004. 18751

Zasetsky, A. Y., Khalizov, A. F., Earle, M. E., and Sloan, J. J.: Frequency dependent complex refractive indices of supercooled liquid water and ice determined from aerosol extinction spectra, J. Phys. Chem. A., 109, 2760–2764., 2005. 18751, 18752, 18756, 18762

Zhang, E., Wang, Z., and Liu, D.: A global view of midlevel liquid-layer topped stratiform cloud distribution and phase partition from CALIPSO and CloudSat measurements, J. Geophys. Res., 115, D00H13, doi:10.1029/2009JD012143, 2010. 18750

ACPD
13, 18749–18770, 2013

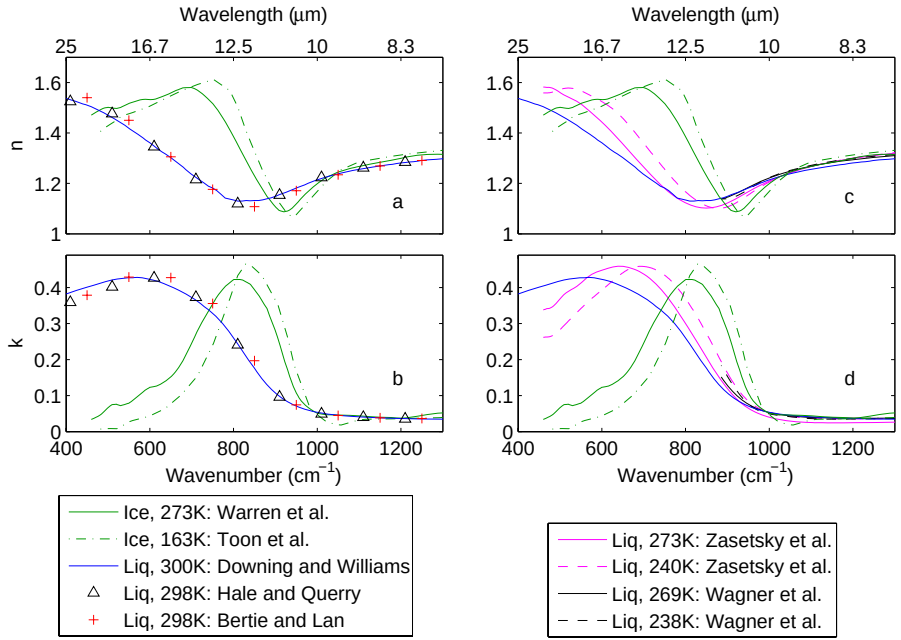

Fig. 1. Measurements of the complex indices of refraction (CRI) of ice and liquid water. Top panels show the real parts of the CRI (n: **a** and **c**), while bottom panels show the imaginary part (k: **b** and **d**). The left panels show the CRI of liquid water for temperatures of 298 K and above (made prior to 1996) while the right panels also include liquid water CRI at temperatures of 273 K and below (made in 2005).

ACPD
13, 18749–18770, 2013

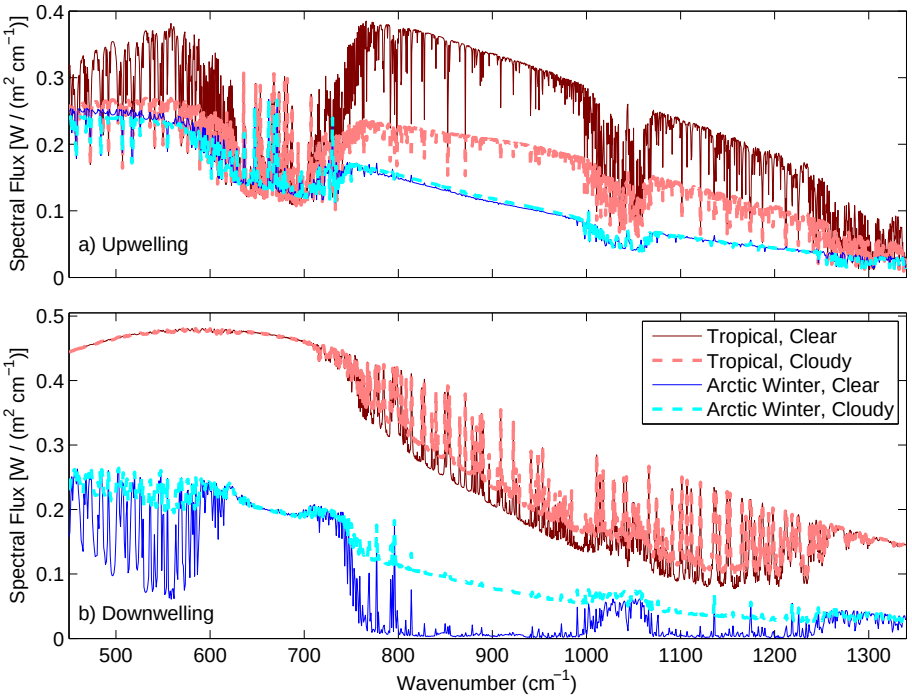

Fig. 2. Spectral fluxes from clear and cloudy skies for a warm/wet extreme model atmosphere (tropical) and a cold/dry extreme model atmosphere (Arctic winter). **(a)** Flux downwelling to the surface and **(b)** Flux upwelling to the top of atmosphere. Plots are on a 1 wavenumber spacing. The model cloud is a single-layer liquid cloud with effective radius of 10 µm, and cloud liquid water path of 8 g m^{-2}, at a temperature of 240 K.

ACPD
13, 18749–18770, 2013

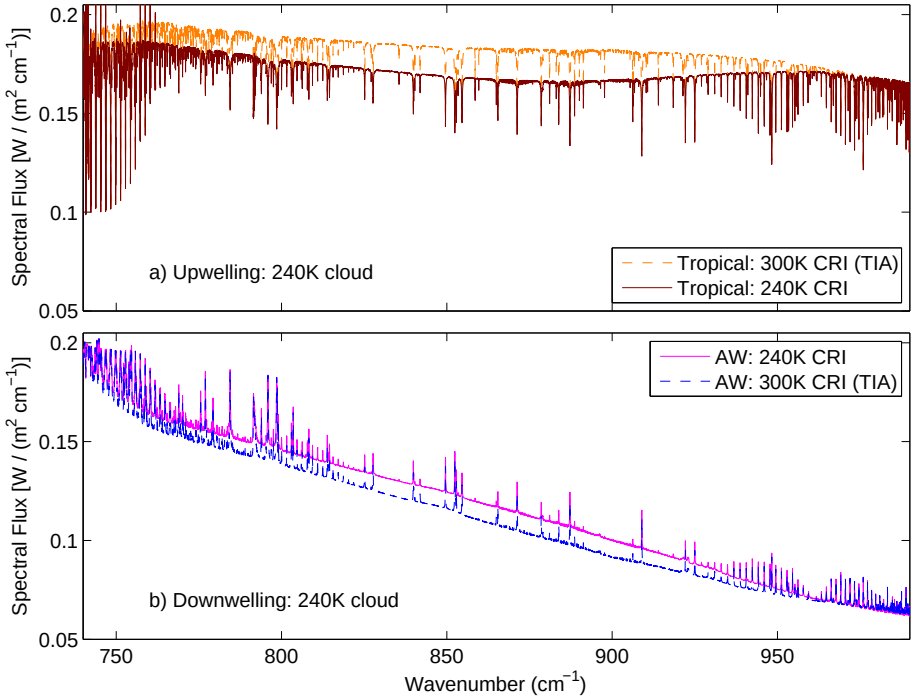

Fig. 3. Spectral flux for a cloudy atmosphere containing a single-layer liquid cloud at 240 K, simulated using complex indices of refraction based on measurements made at 300 K and 240 K. The particle size was 10 µm, and the cloud liquid water path was 8 g m^{-2}. **(a)** Upwelling spectral flux for a tropical atmosphere and **(b)** Downwelling spectral flux for an Arctic winter atmosphere (AW).

ACPD
13, 18749–18770, 2013

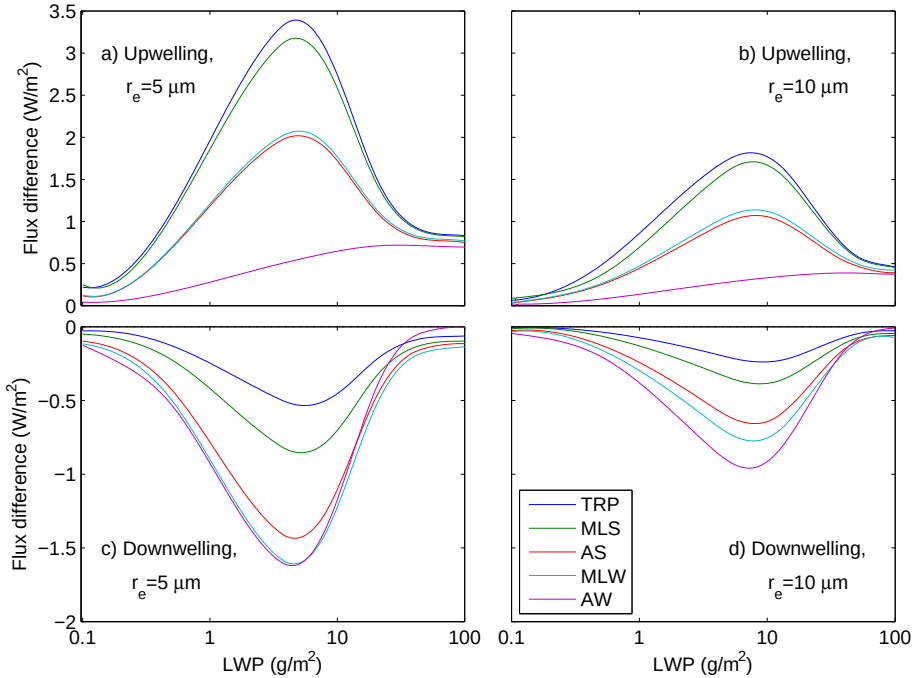

Fig. 4. Difference between flux simulated using 300 K indices of refraction and using 240 K indices of refraction (see text for explanation) as a function of cloud liquid water path (LWP) for single-layer liquid clouds with effective radii (r_e) of 5 and 10 µm in a variety of model atmospheres (Arctic winter: AW, midlatitude winter: MLW, Arctic summer: AS, midlatitude summer: MLS, and tropical: TRP), for upwelling flux at the top of atmosphere (**a** and **b**) and downwelling flux at the surface (**c** and **d**).

ACPD
13, 18749–18770, 2013

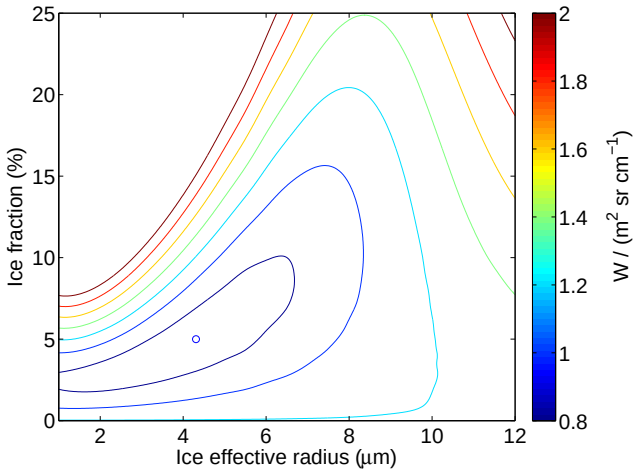

Fig. 5. Error contours of the root mean square difference between simulated and "measured" atmospheric radiances, where both are based on model radiances at selected frequencies, for a 240 K liquid-only cloud with a liquid water path of 8 g m^{-2} and effective radius of 10 μm. The color bar gives the error contour values, in mW (m^2 sr cm^{-1})$^{-1}$. The circle marks the minimum.

ACPD
13, 18749–18770, 2013